The Dynamic Indium-Bridged [1.1]Ferrocenophane $[(Me_2Ntsi)In(C_5H_4)_2Fe]_2$

Jörg A. Schachner,[‡,⊥] Clinton L. Lund,[‡] Ian J. Burgess,[‡] J. Wilson Quail,[§] Gabriele Schatte,[§] and Jens Müller*[,‡]

Department of Chemistry and Saskatchewan Structural Sciences Centre, University of Saskatchewan, 110 Science Place, Saskatoon, Saskatchewan S7N 5C9, Canada

Received April 16, 2008

Salt metathesis reaction between Li(thf)(Me_2Ntsi) [Me_2Ntsi = $C(SiMe_3)_2SiMe_2NMe_2$] and InX_3 gave the new indium dihalides (Me_2Ntsi)InX_2 [X = Cl (**2a**), I (**2b**); isolated yields 34% (**2a**) and 44% (**2b**)]. Single-crystal X-ray analysis revealed that **2a** is a Cl-bridged dimer, while **2b** is monomeric. Salt metathesis reaction between dilithioferrocene and **2a** and **2b**, respectively, gave the new indium-bridged [1.1]ferrocenophane [(Me_2Ntsi)In(η^5-C_5H_4)$_2$Fe]$_2$ (**3**). Only when **2a** was used, could analytically pure **3** be isolated (45%). Revealed by a single-crystal X-ray analysis, compound **3** crystallized as an *anti* isomer (C_i symmetry). The diinda[1.1]ferrocenophane **3** showed fluxional behavior in solution. The proton NMR spectrum of **3** revealed only five singlets at ambient temperature (500 MHz, 25 °C, C_6D_6 or C_7D_8): one singlet for $SiMe_2$, $SiMe_3$, and NMe_2 each and two singlets for the 16 Cp protons. These facts can be rationalized by assuming a fast degenerate isomerization from one *anti* isomer to another *anti* isomer (time-averaged D_{2h} symmetry). The two singlets at 4.43 and 4.45 ppm (500 MHz, 25 °C, C_7D_8) of the α- and β-protons broadened at lower temperature and coalesced at 5 °C. By lowering the temperature further, two sets of signals emerged and became clearly visible at −30 °C, with each set consisting of four singlets for the Cp protons of equal intensity. Consistent with the splitting of the Cp signals, all other signals split in two sets of three singlets, indicating C_s symmetric Me_2Ntsi moieties. These data show that the [1.1]ferrocenophane **3** exists as a mixture of two isomers in toluene solutions (2:1 ratio at −30 °C). Assuming that the thermodynamically favored isomer was found in the crystal lattice, the most intense set of signals was assigned to the *anti* isomer of **3**, while the less intense set of signals was assigned to a *syn* isomer. The already known diinda[1.1]ferrocenophane {[2-(Me_2NCH_2)C_6H_4]In(η^5-C_5H_4)$_2$Fe}$_2$ (**1c**) was revisited. Compound **1c** did not reveal any fluxional behavior in 1D ^{1}H NMR spectra at ambient temperature, but EXSY spectroscopy revealed an occurring *anti*-to-*anti* isomerization of **1c** in solution. A cyclic voltammogram of **3** in thf/0.1 M [Bu_4N][PF_6] showed only an irreversible oxidation. A rationale is given why the reaction of (Me_2Ntsi)InX_2 [X = Cl (**2a**), I (**2b**)] with dilithioferrocene gave a [1.1]ferrocenophane, as similar reactions of (Me_2Ntsi)ECl_2 (E = Al, Ga) with dilithioferrocene gave strained [1]ferrocenophanes.

Introduction

[1.1]Ferrocenophanes stepped on the scientific stage when Nesmeyanov and Kritskaya described the first example in 1956 (Figure 1; ER_x = CH_2, CHPh).[1] [1.1]Ferrocenophanes with carbon in bridging positions prefer the *syn* conformation (Figure 1; E = C);[2] however, an *anti* isomer was structurally characterized for the first time in 1993.[3]

Since the synthesis of the first heteroatom-bridged [1.1]ferrocenophane, a $SnBu_2$-bridged species,[4] this family of ferrocene derivatives has grown significantly. To date, [1.1]ferrocenophanes of boron,[5] aluminum,[6–8] gallium,[8,9] indium,[8] silicon,[10,11] tin,[4,12] lead,[13] phosphorus,[14–16] sulfur,[17] and mercury[18] are described in the literature. The chemistry of [1.1]ferrocenophanes had been extended to ruthenium: besides reports about carbon-bridged [1.1]ruthenocenophanes and mixed Ru−Fe [1.1]metallocenophanes,[2] to the best of our knowledge, a $SiMe_2$-bridged species[11] is the only heteroatom-bridged [1.1]ruthenocenophane to date. These [1.1]metallacyclophanes are formal

* Corresponding author. E-mail: jens.mueller@usask.ca.
‡ Department of Chemistry.
§ Saskatchewan Structural Sciences Center.
⊥ Current address: Department of Chemistry, University of British Columbia, 6174 University Blvd., Vancouver, British Columbia V6T 1Z3, Canada.

(1) Nesmeyanov, A. N.; Kritskaya, I. I. *Bull. Acad. Sci. USSR, Div. Chem. Sci. (Eng. Transl.)* **1956**, *24*, 243–244.
(2) Mueller-Westerhoff, U. T. *Angew. Chem., Int. Ed. Engl.* **1986**, *25*, 702–717.
(3) Löwendahl, M.; Davidsson, Ö.; Ahlberg, P.; Håkansson, M. *Organometallics* **1993**, *12*, 2417–2419.
(4) (a) Seyferth, D.; Withers, H. P. *Organometallics* **1982**, *1*, 1275–1282. (b) Clearfield, A.; Simmons, C. J., Jr.; Seyferth, D. *Inorg. Chim. Acta* **1983**, *75*, 139–144.
(5) Scheibitz, M.; Winter, R. F.; Bolte, M.; Lerner, H.-W.; Wagner, M. *Angew. Chem., Int. Ed.* **2003**, *42*, 924–927.
(6) Braunschweig, H.; Burschka, C.; Clentsmith, G. K. B.; Kupfer, T.; Radacki, K. *Inorg. Chem.* **2005**, *44*, 4906–4908.
(7) Schachner, J. A.; Lund, C. L.; Quail, J. W.; Müller, J. *Acta Crystallogr.* **2005**, *E61*, m682–m684.
(8) Schachner, J. A.; Orlowski, G. A.; Quail, J. W.; Kraatz, H.-B.; Müller, J. *Inorg. Chem.* **2006**, *45*, 454–459.
(9) (a) Jutzi, P.; Lenze, N.; Neumann, B.; Stammler, H. G. *Angew. Chem., Int. Ed.* **2001**, *40*, 1424–1427. (b) Uhl, W.; Hahn, I.; Jantschak, A.; Spies, T. *J. Organomet. Chem.* **2001**, *637*, 300–303. (c) Althoff, A.; Jutzi, P.; Lenze, N.; Neumann, B.; Stammler, A.; Stammler, H.-G. *Organometallics* **2002**, *21*, 3018–3022. (d) Althoff, A.; Jutzi, P.; Lenze, N.; Neumann, B.; Stammler, A.; Stammler, H. G. *Organometallics* **2003**, *22*, 2766–2774. (e) Althoff, A.; Eisner, D.; Jutzi, P.; Lenze, N.; Neumann, B.; Schoeller, W. W.; Stammler, H.-G. *Chem.−Eur. J.* **2006**, *12*, 5471–5480.

10.1021/om800342e CCC: $40.75
Publication on Web 08/19/2008

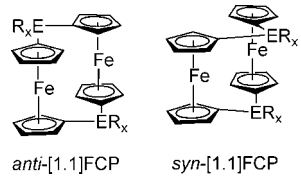

Figure 1. Two different isomers of [1.1]ferrocenophanes.

dimers of strained [1]metallacyclophanes, which are prone to ring-open polymerize to produce new organometallic materials.[19]

In the course of our investigation of aluminum- or gallium-bridged metallacyclophanes, we discovered that the bulkiness of the ligand that is attached to the bridging group-13 element plays a crucial role. When the bulky *trisyl*-based ligands Pytsi or Me_2Ntsi (Figure 2) were applied, strained [1]metallacyclophanes were formed;[20–24] the use of the slimmer "one-armed phenyl" ligand Ar′ or p-*t*BuAr′ (Figure 2) resulted in unstrained [1.1]metallacyclophanes.[6,8,25] Among the latter species are the first [1.1]metallacyclophanes of bis(benzene) complexes, i.e., aluminum- and gallium-bridged [1.1]chromarenophanes and [1.1]molybdarenophanes (Figure 3).[25]

Strained [1]metallacyclophanes with indium in bridging positions are unknown. Our first attempt to get access to an inda[1]ferrocenophane by reacting (Pytsi)$InCl_2$ with dilithioferrocene resulted only in the isolation of the 1,1′-disubstituted ferrocene derivative [{(Pytsi)(μ-Cl)In}C_5H_4]$_2$Fe.[21] The reaction of Ar′$InCl_2$ with dilithioferrocene gave the unstrained [1.1]ferrocenophane [(Ar′In)$(C_5H_4)_2$Fe]$_2$ (**1c**; Figure 3), which is the only known diinda[1.1]ferrocenophane to date.

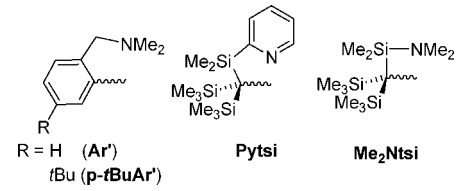

Figure 2. Intramolecularly coordinating ligands used for the synthesis of heavier group-13-bridged metallacyclophanes.

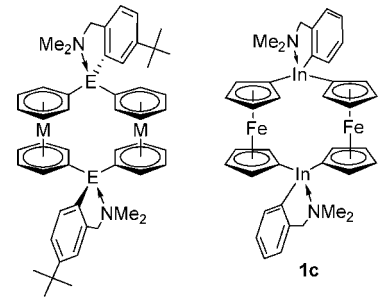

Figure 3. The first [1.1]chromarenophanes (M = Cr; E = Al or Ga) and [1.1]molybdarenophanes (M = Mo; E = Al or Ga)[25] and the first diinda[1.1]ferrocenophane (**1c**).[8]

Within this report, we describe the outcome of another attempt to prepare an indium-bridged [1]ferrocenophane.

Results and Discussion

We attempted the synthesis of an indium-bridged [1]ferrocenophane by following the methods that we successfully implemented for aluminum- and gallium-bridged [1]ferrocenophanes,[22] [1]chromarenophanes,[22] [1]vanadarenophanes,[22] [1]ruthenocenophanes,[23] and [1]molybdarenophanes.[24] In all these cases, the strained metallacyclophane had been synthesized via salt metathesis of dilithiated sandwich complexes with aluminum or gallium dichlorides; the bridging group-13 element was always equipped with the bulky, intramolecularly coordinating Me_2Ntsi ligand (Figure 2). In order to apply this method to indium, we first needed to prepare respective indium dihalides.

Preparation and Characterization of Indium Dihalides 2a and 2b. Salt metathesis reaction between Li(thf)(Me_2Ntsi) and $InCl_3$ and InI_3 gave the new indium dihalides **2a** and **2b**, respectively (eq 1). Both compounds were isolated as analytically pure species through crystallization in moderate yields of 34% (**2a**) and 44% (**2b**), respectively.

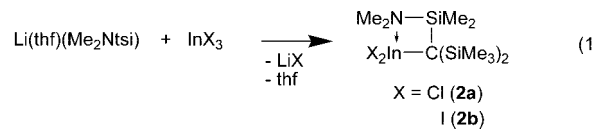

(1)

Their molecular structures have been determined by single-crystal X-ray structural analysis (Figures 4 and 5; Table 1). Compound **2a** is a chlorine-bridged dimer (Figure 4), in which each In atom is in the center of a distorted trigonal bipyramid. Both bipyramids share one edge between an equatorial and an apical Cl atom to give a centrosymmetric dimer with C_i symmetry. A similar centrosymmetric dimer was found for (Pytsi)$InCl_2$ (Figure 2),[21] and therefore, it is not surprising that

(10) (a) Park, J. W.; Seo, Y. S.; Cho, S. S.; Whang, D. M.; Kim, K. M.; Chang, T. Y. *J. Organomet. Chem.* **1995**, *489*, 23–25. (b) Zechel, D. L.; Foucher, D. A.; Pudelski, J. K.; Yap, G. P. A.; Rheingold, A. L.; Manners, I. *J. Chem. Soc., Dalton Trans.* **1995**, 1893–1899. (c) Ni, Y. Z.; Rulkens, R.; Pudelski, J. K.; Manners, I. *Macromol. Rapid Commun.* **1995**, *16*, 637–641. (d) Reddy, N. P.; Choi, N.; Shimada, S.; Tanaka, M. *Chem. Lett.* **1996**, 649–650. (e) MacLachlan, M. J.; Zheng, J.; Thieme, K.; Lough, A. J.; Manners, I.; Mordas, C.; LeSuer, R.; Geiger, W. E.; Liable-Sands, L. M.; Rheingold, A. L. *Polyhedron* **2000**, *19*, 275–289. (f) Calleja, G.; Carré, F.; Cerveau, G. *Organometallics* **2001**, *20*, 4211–4215. (g) Berenbaum, A.; Lough, A. J.; Manners, I. *Organometallics* **2002**, *21*, 4415–4424. (h) Bao, M.; Hatanaka, Y.; Shimada, S. *Chem. Lett.* **2004**, *33*, 520–521.

(11) Herberhold, M.; Bärtl, T. *Z. Naturforsch. B* **1995**, *50*, 1692–1698.

(12) (a) Dong, T. Y.; Hwang, M. Y.; Wen, Y. S.; Hwang, W. S. *J. Organomet. Chem.* **1990**, *391*, 377–385. (b) Jäkle, F.; Rulkens, R.; Zech, G.; Foucher, D. A.; Lough, A. J.; Manners, I. *Chem.−Eur. J.* **1998**, *4*, 2117–2128. (c) Jäkle, F.; Rulkens, R.; Zech, G.; Massey, J.; Manners, I. *J. Am. Chem. Soc.* **2000**, *122*, 4231–4232. (d) Baumgartner, T.; Jäkle, F.; Rulkens, R.; Zech, G.; Lough, A. J.; Manners, I. *J. Am. Chem. Soc.* **2002**, *124*, 10062–10070.

(13) Utri, G.; Schwarzhans, K. E.; Allmaier, G. M. *Z. Naturforsch. B* **1990**, *45*, 755–762.

(14) Brunner, H.; Klankermayer, J.; Zabel, M. *J. Organomet. Chem.* **2000**, *601*, 211–219.

(15) Mizuta, T.; Onishi, M.; Miyoshi, K. *Organometallics* **2000**, *19*, 5005–5009.

(16) Mizuta, T.; Imamura, Y.; Miyoshi, K. *Organometallics* **2005**, *24*, 990–996.

(17) Ieong, N. S.; Chan, W. Y.; Lough, A. J.; Haddow, M. R.; Manners, I. *Chem.−Eur. J.* **2008**, *14*, 1253–1263.

(18) (a) Lemenovskii, D. A.; Urazowski, I. F.; Baukova, T. V.; Arkhipov, I. L.; Stukan, R. A.; Perevalova, E. G. *J. Organomet. Chem.* **1984**, *264*, 283–288. (b) Kuzmina, I. G.; Struchkov, Y. T.; Lemenovsky, D. A.; Urazowsky, I. F. *J. Organomet. Chem.* **1984**, *277*, 147–151.

(19) (a) Herbert, D. E.; Mayer, U. F. J.; Manners, I. *Angew. Chem., Int. Ed.* **2007**, *46*, 5060–5081. (b) Bellas, V.; Rehahn, M. *Angew. Chem., Int. Ed.* **2007**, *46*, 5082–5104.

(20) (a) Schachner, J. A.; Lund, C. L.; Quail, J. W.; Müller, J. *Organometallics* **2005**, *24*, 785–787. (b) Schachner, J. A.; Quail, J. W.; Müller, J. *Acta Crystallogr.* **2008**, *E64*, m517.

(21) Schachner, J. A.; Lund, C. L.; Quail, J. W.; Müller, J. *Organometallics* **2005**, *24*, 4483–4488.

(22) Lund, C. L.; Schachner, J. A.; Quail, J. W.; Müller, J. *Organometallics* **2006**, *25*, 5817–5823.

(23) Schachner, J. A.; Tockner, S.; Lund, C. L.; Quail, J. W.; Rehahn, M.; Müller, J. *Organometallics* **2007**, *26*, 4658–4662.

(24) Lund, C. L.; Schachner, J. A.; Quail, J. W.; Müller, J. *J. Am. Chem. Soc.* **2007**, *129*, 9313–9320.

(25) Lund, C. L.; Schachner, J. A.; Burgess, I. J.; Quail, J. W.; Schatte, G.; Müller, J. *Inorg. Chem.* **2008**, *47*, 5992–6000.

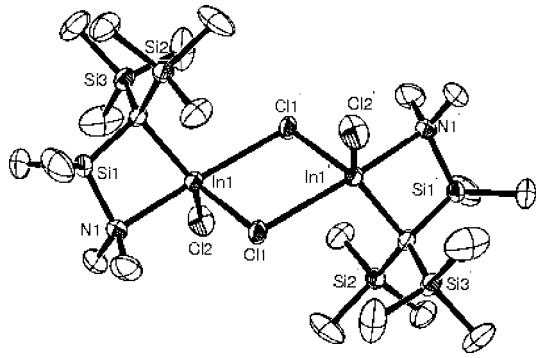

Figure 4. Molecular structure of **2a** with thermal ellipsoids at the 50% probability level (only one of two dimers is shown). Hydrogen atoms are omitted for clarity. Selected bond lengths [Å] and angles [deg]: In1−Cl1 = 2.4521(13), In1−Cl1′ = 2.8363(13), In1−Cl2 = 2.3530(17), In1−C1 = 2.211(5), In1−N1 = 2.385(4), Cl1−In1−C1 = 128.36(14), Cl2−In1−C1 = 127.74(15), Cl1−In1−Cl2 = 103.75(6), N1−In1−Cl1′ = 171.39(12), N1−In1−C1 = 76.83(17), N1−In1−Cl1 = 94.16(11), N1−In1−Cl2 = 97.91(13), Cl1′−In1−C1 = 103.65(14), Cl1′−In1−Cl2 = 88.59(5), Cl1′−In1−Cl1 = 78.75(4). Symmetry transformations used to generate equivalent atoms: $-x+1$, $-y$, $-z+1$.

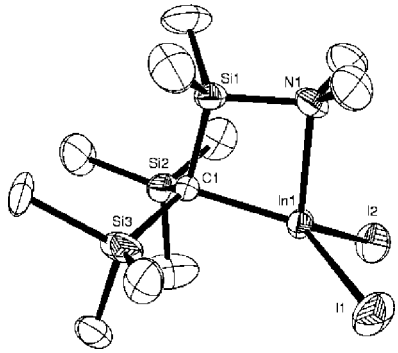

Figure 5. Molecular structure of **2b** with thermal ellipsoids at the 50% probability level. Hydrogen atoms are omitted for clarity. Selected bond lengths [Å] and angles [deg]: In1−I1 = 2.7047(5), In1−I2 = 2.6949(5), In1−N1 = 2.310(4), In1−C1 = 2.215(4), N1−In1−C1 = 78.64(17), N1−In1−I1 = 106.05(12), N1−In1−I2 = 110.65(12), I1−In1−I2 = 103.494(19), I1−In1−C1 = 126.73(12), I2−In1−C1 = 124.86(12).

the two related species, **2a** and (Pytsi)$InCl_2$,[21] show very similar bond lengths and angles. For example, the bond length [Å] for the In_2Cl_4 core of **2a** are (values for (Pytsi)$InCl_2$ in square brackets taken from ref 21) In1−Cl1 = 2.4521(13) [2.4812(7)], In1−Cl1′ = 2.8363(13) [2.7706(7)], and In1−Cl2 = 2.3530(17) [2.3845(7)]. In contrast to the indium chloride **2a**, the corresponding iodide **2b** is a monomer in the solid state (Figure 5), an expected result, based on the known structure of the related compound (Pytsi)InI_2.[26] Again, the Me_2Ntsi-containing species **2b** is not strikingly different compared to its cousin (Pytsi)InI_2.

Compounds **2a** and **2b** show very similar NMR spectra. For example, three singlets in the proton NMR spectra with nearly identical chemical shifts for both species render **2a** and **2b** C_s symmetric in solution on time average. On the basis of these data, one can speculate that the chloride **2a** takes part in a fast monomer−dimer equilibrium, which lies predominantly on the side of the monomer in benzene solutions.

(26) Lund, C. L.; Schachner, J. A.; Quail, J. W.; Müller, J. *Acta Crystallogr.* **2005**, *E61*, m2063–m2065.

Synthesis and Solid-State Structure of Diinda[1.1]ferrocenophane 3. In an earlier attempt to prepare an inda[1]ferrocenophane from [(Pytsi)InCl(μ-Cl)]$_2$ and dilithioferrocene, we could isolate only the 1,1′-disubstituted ferrocene [{(Pytsi)(μ-Cl)In}C_5H_4]$_2$Fe.[21] The indium moieties in this disubstituted ferrocene were bridged by Cl atoms similarly to those of the starting compound [(Pytsi)InCl(μ-Cl)]$_2$. This result left the impression that the dimeric nature of the starting dichloride might prevent the formation of the targeted inda[1]ferrocenophane and that a monomeric starting indium dihalide is required. This was the reason that we synthesized the diiodide **2b** in addition to the dichloride **2a**.

To our surprise, both new indium dihalides react with dilithioferrocene to give a [1.1]ferrocenophane (**3**) and not the targeted [1]ferrocenophane (eq 2). However, the isolation of pure **3** turned out to be difficult in both cases, and analytically pure product was obtained only from reactions with the dichloride **2a** through crystallization from toluene solutions (yield of 45%).

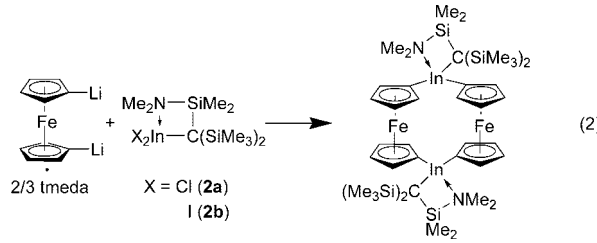

(2)

The [1.1]ferrocenophane **3** crystallizes in the monoclinic space group $P2_1/c$ (Table 1) as a centrosymmetric *anti* isomer (Figures 6 and 1). The geometry around each In atom can be best described as a flattened trigonal pyramid with C1, C10, and C11 forming the base and N1 at the apex of the pyramid. The sum over the three C−In−C angles of 359.6° indicates that the In atom is almost part of the plane defined by the three C atoms. The In1−N1 bond axis is tilted away from the ferrocene unit, which can be illustrated by the acute angle of 75.09(14)° for C11−In1−N1. The longest bond around indium is the In1−N1 donor bond at 2.437(3) Å. Compound **3** can be best compared to the only other known indium-bridged [1.1]ferrocenophane **1c** (Figure 3), which is equipped with the Ar′ instead of the Me_2Ntsi ligand (Figure 2).[8] The In atoms of **1c** are coordinated similarly to those in **3**; however, the trigonal pyramid is, with a sum of 358.0° over the three C−In−C angles, slightly less flattened than that in compound **3**. Furthermore, the acute C−N−C angle of 77.99(15)° is larger and the In−N bond length of 2.386(4) Å is shorter compared to species **3**.[8] The differences between **1c** and **3** might be mainly a consequence of different ring sizes of the indium-containing cycles: a five-membered compared to a four-membered ring. Presumably, the higher strained four-membered cycle in compound **3** does not allow for an ideal orbital overlap between nitrogen and indium, with the consequence of a lengthened and, hence, weaker In−N donor bond in **3** compared to that of **1c**.

NMR Spectroscopy of Diinda[1.1]ferrocenophane 3. The proton NMR spectrum of **3** shows only five singlets: one singlet for each of the $SiMe_2$, $SiMe_3$, and NMe_2 moieties and two singlets for the 16 Cp protons[27] (Figure S1, Supporting

(27) Often the Cp protons appear as pseudotriplets; however, in the case of **3**, the triplet structure is not resolved and they appear as singlets.

(28) Löwendahl, J.-M.; Håkansson, M. *Organometallics* **1995**, *14*, 4736–4741.

Table 1. Crystal and Structural Refinement Data for Compounds 2a, 2b, and 3

	$(2a)_2$	2b	3
empirical formula	$C_{22}H_{60}Cl_4In_2N_2Si_6$	$C_{11}H_{30}I_2InNSi_3$	$C_{42}H_{76}Fe_2In_2N_2Si_6$
fw	892.70	629.25	1118.93
cryst size/mm^3	0.17 × 0.15 × 0.13	0.20 × 0.20 × 0.20	0.10 × 0.04 × 0.02
cryst syst, space group	triclinic, $P\bar{1}$	monoclinic, $P2_1/c$	monoclinic, $P2_1/c$
Z	2	4	2
a/Å	11.0773(4)	8.3419(2)	17.1413(4)
b/Å	12.7834(5)	17.9380(6)	9.5085(3)
c/Å	14.8553(5)	16.5700(4)	16.7639(5)
α/deg	83.170(3)	90	90
β/deg	89.900(3)	116.6581(17)	112.1530(10)
γ/deg	79.024(2)	90	90
volume/Å^3	2049.99(13)	2215.91(11)	2530.62(12)
ρ_{calc}/mg/m^3	1.446	1.886	1.468
temperature/K	173(2)	173(2)	173(2)
μ_{calc}/mm^{-1}	1.577	4.005	1.634
θ range/deg	2.71 to 26.37	2.70 to 27.48	2.45 to 26.37
no. of reflns collected	27 183	8715	40 374
no. of indep/obsd reflns	8358/6532	5039/4282	5170/3917
absorp corr	ψ-scan	multiscan	ψ-scan
no. of data/restraints/params	8358/0/350	5039/21/204	5170/0/254
goodness-of-fit on F^2	1.074	1.069	1.052
R_1 indices $[I > 2\sigma(I)]^a$	0.0500	0.0423	0.0437
wR_2 (all data)^a	0.1250	0.1044	0.0929
largest diff peak and hole, $\Delta\sigma_{elect}$/Å^{-3}	2.838 and −0.749	1.175 and −1.605	0.632 and −0.999

^{a} $R_1 = [\sum||F_o| - |F_c||]/[\sum|F_o|]$ for $[F_o^2 > 2\sigma(F_o^2)]$, $wR_2 = \{[\sum w(F_o^2 - F_c^2)^2]/[\sum w(F_o^2)^2]\}^{1/2}$ [all data].

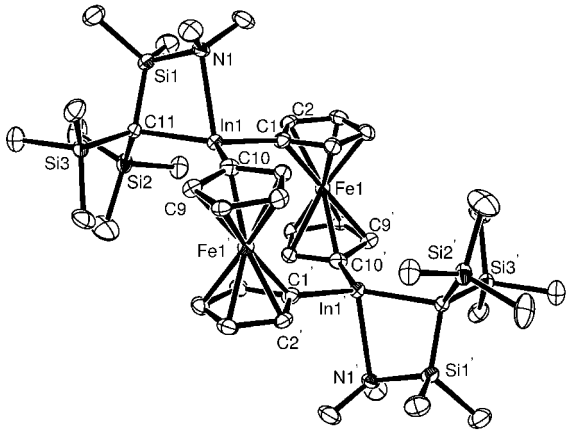

Figure 6. Molecular structure of **3** with thermal ellipsoids at the 50% probability level. H atoms are omitted for clarity. Selected bond lengths [Å] and angles [deg]: In1−N1 = 2.437(3), In1−C1 = 2.173(4), In1−C10 = 2.160(5), In1−C11 = 2.291(4), Fe1−Fe1′ = 5.490(1), C1−In1−C10 = 113.07(17), C1−In1−C11 = 125.39(17), C10−In1−C11 = 121.09(17), C1−In1−N1 = 96.96(14), C10−In1−N1 = 106.29(15), C11−In1−N1 = 75.09(14).

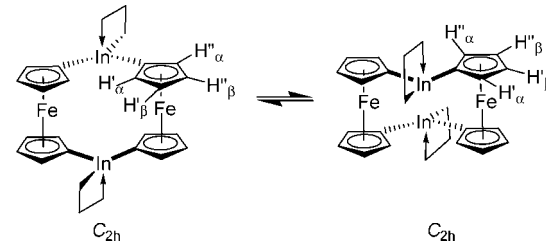

Figure 7. Illustration of an *anti*-to-*anti* degenerate isomerization of **3**. Inner Cp protons of the left molecule (H′$_\alpha$ and H′$_\beta$) are converted into outer Cp protons of the right molecule (H′$_\alpha$ and H′$_\beta$) and vice versa.

Information). The fact that all Cp protons result in only two singlets directly reveals the presence of a 2-fold symmetry element that renders the two halves of the monosubstituted C_5H_4 moieties equivalent. In the solid state, however, compound **3** exhibits C_i symmetry, and one would expect that the folded four-membered rings invert fast in solution, resulting in a time-averaged C_{2h} symmetric species. Such a species would give four peaks for the C_5H_4 moieties: two for the inner protons (H_α and H_β) and two for the outer protons (H_α and H_β). A [1.1]ferrocenophane in an *anti* conformation (Figure 1) can be looked upon as an expanded cyclohexane in a chair conformation; an *anti*-to-*anti* isomerization in [1.1]ferrocenophanes is equivalent to a chair-to-chair isomerization in cyclohexane.[2,28] If such a degenerate isomerization would occur fast for compound **3** on the NMR time scale, D_{2h} symmetry would result on time average. This process is illustrated in Figure 7, where it is shown that inner Cp protons are converted into outer Cp protons and vice versa. Furthermore, this isomerization leads to identical molecules only if breakage of the In−N donor bonds, rotation of the Me_2Ntsi ligands around In−C bonds, and formation of an In−N donor bond on the opposite side of both In atoms are involved. This proposed *anti*-to-*anti* isomerization can explain the measured NMR spectra of species **3** at ambient temperature.

In order to get further insight into the fluxional behavior of the [1.1]ferrocenophane **3**, proton NMR spectra were recorded at low temperatures (25 to −80 °C). Figure 8 depicts the Cp range of selected ^{1}H NMR spectra between 25 and −30 °C. The two singlets at 4.43 and 4.45 ppm (25 °C) of the α- and β-protons broaden at lower temperature and coalesce at 5 °C. By lowering the temperature further, two sets of signals emerge and become clearly visible at −30 °C, with each set consisting of four singlets of equal intensity. Consistent with the splitting of the Cp signals, all other signals split in two sets of three singlets, indicating C_s symmetric Me_2Ntsi moieties (Figure S2, Supporting Information). These data clearly show that the [1.1]ferrocenophane **3** exists as a mixture of two isomers in toluene solutions in a 2:1 ratio at −30 °C. Assuming that the thermodynamically favored isomer was found in the crystal lattice, we assigned the most intense set of signals to the *anti* isomer of **3**. The second set of signals can be assigned to the *syn* isomer of **3**, as the minor component. With *syn* isomer we mean an isomer in which the (Me_2Ntsi)In moieties are both on the same side of the two ferrocene units (Figure 1). In analogy with cyclohexane, such an isomer could be similar to either a twist-boat or a boat conformation, the latter being a transition

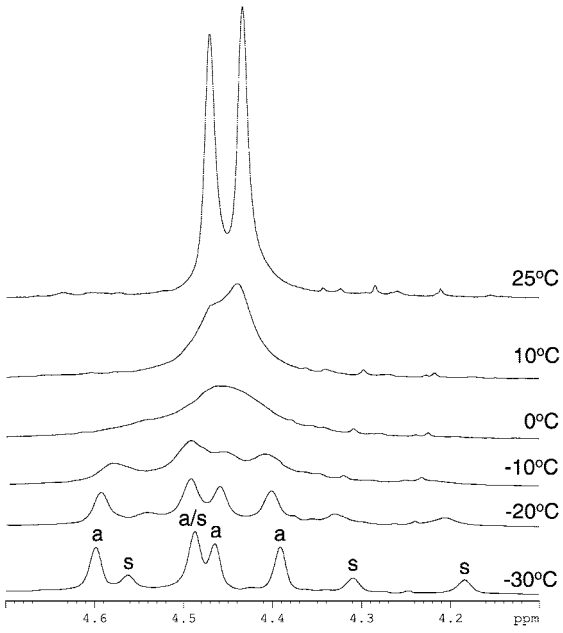

Figure 8. Cp region of selected ^{1}H NMR spectra of compound **3** (500 MHz; toluene-d_8). Indication "a" refers to the *anti* isomer of **3**; indication "s" refers to the *syn* isomer of **3** (see text for discussion); "a/s" indicates two coincidently overlapping peaks.

state for a twist-boat-to-twist-boat isomerization of cyclohexane. On the basis of the experimental evidence, it is impossible to prove the exact nature of the minor isomer of compound **3**. It might be that the minor isomer has a similar structure to a twist-boat conformation of cyclohexane (D_2 symmetry). Compound **3** in a twist-boat conformation would exhibit C_2 symmetry, but one can assume that both enantiomers equilibrate fast on the NMR time scale, resulting in a time-averaged C_{2v} symmetrical *syn* isomer. In summary, the *anti* and the *syn* both should give the same number of signals with a similar pattern, and that is what was found experimentally.

Further support for this interpretation comes from published knowledge of the dynamic behavior of other [1.1]ferrocenophanes. Most of the carbon-bridged [1.1]ferrocenophanes were found as *syn* isomers; however, in 1993 an *anti* isomer was structurally characterized for the first time (Figure 1; ER_x = CHMe).[3] Because of their dynamic behavior in solution, [1.1]ferrocenophanes have been coined "molecular acrobats".[2,28,29] With the exception of phosphorus,[15,16] boron,[5] and the recently published dithia[1.1]ferrocenophane,[17] all other heteroatom-bridged [1.1]ferrocenophanes crystallize as *anti* isomers. Interestingly, for a Ph(S)P-bridged [1.1]ferrocenophane, both isomers could be characterized by single-crystal X-ray analysis.[16] For the desulfurized [1.1]ferrocenophane (Figure 1; ER_x = PhP), only the *syn* isomer crystallized, but both isomers were synthesized and form an equilibrium in toluene solutions.[16] However, the conversion from the *anti* to the thermodynamically preferred *syn* isomer requires heating, which is in contrast to fast *syn*−*anti* equilibria known for carbon-bridged species.[2,28,29] The authors rationalize the slow conversion by the fact that it requires an inversion of one of the two bridging phosphorus atoms.[16]

As already mentioned before, the first diinda[1.1]ferrocenophane (**1c**) was described recently.[8] Similar to its aluminum[6,8] and gallium[8] counterparts, it crystallized as an *anti* isomer. ^{1}H and

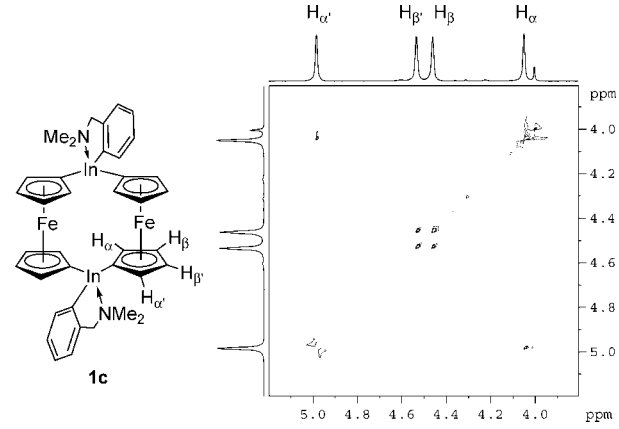

Figure 9. (Left) Assignment of Cp protons in **1c** by NOE experiments. (Right) Cp region of an EXSY spectrum of **1c** (small signal at 3.99 ppm corresponds to ferrocene).

^{13}C NMR spectra could be interpreted as being caused by C_{2h} symmetrical molecules, a finding consistent with the structure of **1c** in the solid state; dynamic behavior was not revealed by these one-dimensional NMR spectra. An emerging second signal set at −80 °C in the ^{1}H NMR spectra hinted toward the presence of a second isomer;[8] however, peaks were too broad to be resolved and the identity of the second isomer could not be illuminated. Against the background of the high flexibility of the indium species **3**, we re-examined compound **1c** (Figure 9). With a series of NOE measurements all four Cp protons could be assigned to NMR signals. The EXSY spectrum of **1c** reveals, with cross-peaks between both α- and both β-protons, that the inner protons exchange their positions with the outer protons, which clearly reveals an *anti*-to-*anti* isomerization of **1c** in solution.

Cyclic Voltammetry of Diinda[1.1]ferrocenophane 3. [1.1]Ferrocenophanes can serve as model compounds to investigate the communication between two linked redox-active metal atoms. Usually, heteroatom-bridged [1.1]ferrocenophanes show two one-electron redox couples, indicating weak interactions of the two iron atoms (class II species).

We attempted to characterize the electrochemical behavior of compound **3** using cyclic voltammetry and 0.1 M $[Bu_4N][PF_6]$ in dry thf as an electrolyte. The resulting voltammogram (Figure 10) displays a pronounced oxidation wave at approximately 1 V versus the formal potential of ferrocene. However, this process is completely irreversible, as there is no evidence of a reduction half-reaction in the cathodic sweep. We have recently reported somewhat similar electrochemical behavior for an aluminum-bridged [1.1]ferrocenophane where both a reversible redox couple and an irreversible wave at more positive potentials were observed.[8] Quartz crystal microbalance studies of that system clearly demonstrated that the irreversible oxidation led to the formation of a passivating film on the working electrode. This is quite consistent with our present work, where we observe a steady decrease in the oxidation current upon repeated potential cycling. If our electrode was removed from the cell, mechanically polished, and then returned to the cell, the first potential cycle was identical to the original scan. Unfortunately, unlike our previous electrochemical studies,[8,25] there are no reversible redox couples in the CV of the diinda[1.1]ferrocenophane **3**. For completeness we would like to indicate that additional CV studies of **3** in thf/0.1 M $[Bu_4N][ClO_4]$ revealed a startling dependence on the nature of the electrolyte's anion. In this electrolyte, compound **3** exhibited a quasi-reversible redox couple with an apparent formal potential of ∼0.1 V vs Fc/Fc^+

(29) Löwendahl, M.; Davidsson, Ö.; Ahlberg, P. *J. Chem. Res., Synop.* **1993**, 40–41.

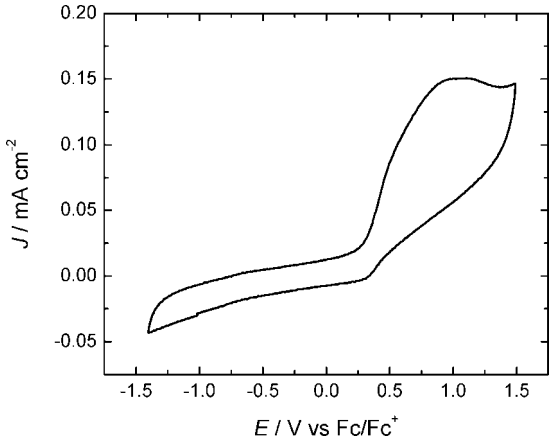

Figure 10. Cyclic voltammogram of **3** in thf/0.1 M $[Bu_4N][PF_6]$ using a glassy carbon working electrode at a scan rate of 100 mV/s. The potential was measured versus a silver quasi-reference electrode and subsequently rereferenced to the formal potential of ferrocene in 0.1 M $[Bu_4N][PF_6]$.

and no evidence of the irreversible wave at positive potentials (Figure S3, Supporting Information). However, the similarity of this CV to the voltammogram of pure ferrocene/ferrocenium and the absence of the redox couple in 0.1 M $[Bu_4N][PF_6]$ is quite suspicious. It seems that either the perchlorate ion or perhaps trace amount of chloride ions led to a degradation of the metallocenophane into a ferrocene-like compound.

Conclusion

The new diinda[1.1]ferrocenophane **3** was obtained by reaction of dilithioferrocene with an indium dihalide $(Me_2Ntsi)InX_2$ (**2a** or **2b**; eq 2). Compound **3** is only the second known indium-bridged [1.1]ferrocenophane to date. The diinda[1.1]ferrocenophane **3** is fluxional in solution, and its NMR spectra at room temperature can be interpreted by assuming a fast degenerate *anti*-to-*anti* isomerization. Upon cooling to −30 °C, the proton NMR spectrum reveals two similar signal patterns, indicating the presence of an *anti*- and a *syn* isomer of **3**. [1.1]Ferrocenophanes are known to be highly dynamic in solutions, and some carbon-bridged species were thoroughly investigated.[2,28] Most of the heteroatom-bridged [1.1]ferrocenophanes show fast degenerate isomerizations; however, to the best of our knowledge, VT NMR measurements had only been applied to a lead-bridged [1.1]ferrocenophane (Figure 1, $ER_x = PbPh_2$).[13] This diplumba[1.1]ferrocenophane, which was assumed to crystallize as an *anti* isomer, showed a significant broadening of one of the two Cp proton signals at −89 °C (300 MHz; CD_2Cl_2), but a coalescence temperature could not be reached.[13]

Recently, we had shown that the steric requirements of the ligand that is attached to the group-13 element plays an important role for aluminum- and gallium-bridged metallacyclophanes. While the bulky *trisyl*-based ligands Pytsi and Me_2Ntsi (Figure 2) stabilized strained [1]metallacyclophanes,[20–24] the slimmer "one-armed phenyl" ligand Ar′ or p-*t*BuAr′ (Figure 2) resulted exclusively in unstrained [1.1]metallacyclophanes (Figure 3).[6,8,25] Against this background it was a surprise that a [1.1]ferrocenophane (**3**) instead of an expected [1]ferrocenophane was formed (eq 2). How can this result be rationalized?

Figure 11 illustrates steric interactions of a Me_2Ntsi moiety in a [1.1]ferrocenophane and a [1]ferrocenophane. The drawings are based on the crystallographic data of compound **3** (left side) and that of the published galla[1]ferrocenophane $[(Me_2Ntsi)Ga(\eta^5\text{-}C_5H_4)_2Fe]$[22] (right side). In both types of compounds the closest H···H contacts[30] are found between the α-H atoms of the ferrocene moieties and Me groups of the Me_2Ntsi ligand (double-headed arrows in Figure 11). If these types of steric repulsions are reduced or even absent, which presumably is the case for Ar′- or p-*t*BuAr′-containing species (Figures 2 and 3), then the unstrained [1.1]metallacyclophane is formed as the thermodynamically preferred species.[6,8,25] However, for a 4-fold-coordinated group 13 element in a bridging position there is less space available around that element in a [1.1]metallacyclophane compared to a [1]metallacyclophane. Therefore, if the bulkiness of ligands starts playing a role, then a [1.1]metallacyclophane is thermodynamically disfavored over a [1]metallacyclophane. These speculations are based on the observation that Pytsi- and Me_2Ntsi-equipped Al and Ga moieties exclusively yielded [1]metallacyclophanes;[20–24] [1.1]metallacyclophanes were not formed. Aluminum and gallium have nearly the same covalent radii (1.25 and 1.26 Å), whereas indium (1.44 Å) is significantly larger (singly bonded, 3-fold-coordinated elements).[31] This increase in size translates into significant longer E−C bonds for indium species, as evident from a comparison of the three In−C bond lengths of 2.173(4) (In1−C1), 2.160(5) (In1−C10), and 2.291(4) Å (In1−C11) for **3** compared with the respective values of 2.008(3), 2.017(3), and 2.048(3) Å for the galla[1]ferrocenophane $[(Me_2Ntsi)Ga(\eta^5\text{-}C_5H_4)_2Fe]$[22] (Figure 11). The longer the E−C bonds are, the weaker the steric repulsion between the ligand and the α-H atoms, with the result that for the $(Me_2Ntsi)E$ bridging moiety with E = In the unstrained [1.1]ferrocenophane but with E = Al[22] or Ga[22] strained [1]ferrocenophanes are the thermodynamically favored species. All these arguments are based on proposed thermodynamic stabilities of [1]metallacyclophanes compared to [1.1]metallacyclophanes. All Al- and Ga-bridged metallacyclophanes were prepared through salt metathesis reactions, and one must assume that these are not equilibrium reactions, which means that the formation of a particular product is kinetically controlled. With respect to the formation of ferrocenophanes from intramolecularly stabilized group-13 dichlorides $RECl_2$, the first intermediate will be an asymmetrically substituted ferrocene in which one Cp ring carries the group-13 element moiety RECl, while the other Cp ring is still lithiated. An *intramolecular* reaction will result in a [1]ferrocenophane, whereas further *intermolecular* reactions will lead to a [1.1]ferrocenophane. Both these reaction routes will involve nucleophilic substitutions of Cl^- by a $C_5H_4^-$, which is a part of a ferrocene derivative, and one can assume that for the rate-determining steps steric interactions between α-H atoms and intramolecularly coordinating ligands (Figure 2) play a key role. That means the same arguments used for the ground-state structures (Figure 11) can be used for transition states.

Experimental Section

General Procedures. All manipulations were carried out using standard Schlenk techniques, if not noted differently. Solvents were dried using an MBraun solvent purification system and stored under nitrogen over 4 Å molecular sieves. C_6D_6 and C_7D_8 were prepared through freeze−pump−thaw procedures and stored under nitrogen over 4 Å molecular sieves. ^1H and ^{13}C NMR spectra were recorded

(30) H···H distances are only taken as an indication of possible steric interactions. The absolute values are not important, as they do not reflect the real H···H distances; however, the comparison of H···H distances in two similar structures is meaningful.

(31) *Holleman-Wiberg Inorganic Chemistry*, 1st English ed.; Academic Press: San Diego, 2001; p 1756.

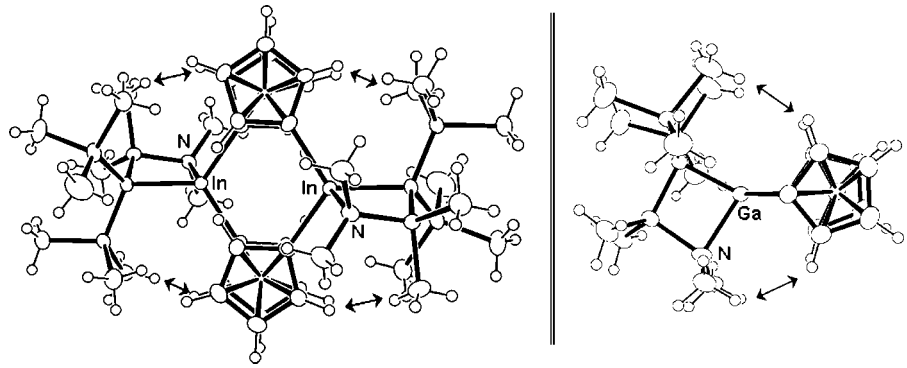

Figure 11. Illustration of the proximity between methyl groups of the Me_2Ntsi ligand and α-protons of the ferrocene moieties (double-headed arrows) in the diinda[1.1]ferrocenophane **3** (left) and the galla[1]ferrocenophane [$(Me_2Ntsi)Ga(\eta^5\text{-}C_5H_4)_2Fe$][22] (right). H···H distances[30] in **3** are 2.15, 2.35, 2.36, and 2.38 Å ($SiMe_3$---αH); H···H distances[30] in [$(Me_2Ntsi)Ga(\eta^5\text{-}C_5H_4)_2Fe$] are 2.28 and 2.44 Å ($SiMe_3$···α-H) and 2.35 and 2.53 Å (NMe_2···α-H).

on a Bruker 500 MHz Avance spectrometer at 25 °C, unless noted differently. ^{1}H chemical shifts were referenced to the residual protons of the deuterated solvent (C_6D_6, δ 7.15; C_7D_8, δ 2.10); ^{13}C chemical shifts were referenced to δ 128.00 (C_6D_6). Mass spectra were measured on a VG 70SE and were reported in the form M (%I) [F], where M is the mass observed, %I is the intensity of the peak relative to the most intense peak in the spectrum, and F is the molecular ion or fragment. Mass peaks with intensities of >10% are reported. Elemental analyses were performed on a Perkin-Elmer 2400 CHN elemental analyzer; samples were prepared in a glovebox, and V_2O_5 was added to promote combustion.

The following compounds were purchased and use as received: $InCl_3$ (99.99%; Alfa Aesar), InI_3 (99.999%; Alfa Aesar), and MeLi (1.0 M in thf/cumene; Aldrich). Li(thf)(Me_2Ntsi) was either freshly prepared, as in the case of **2a**, or isolated through crystallization, as in the case of **2b**.[32] The acronym Me_2Ntsi stands for [$(Me_2N)Me_2Si$]$(Me_3Si)_2C$ (Figure 2). [$(LiC_5H_4)_2Fe$]·$^2/_3$tmeda was synthesized as described in the literature.[33]

Compound **1c** was investigated by NMR exchange spectroscopy (EXSY) (Figure 9). First, a series of gradient 1D NOESY experiments were conducted to assign each peak in the Cp range to a proton. Then the relaxation times T_1 of the Cp protons were measured in order to optimize the mixing times for the EXSY experiment.[34] Relaxation times for the Cp protons were in the range 0.8−1.0 s. Then a series of 2D NOE experiments with mixing times (d_2) of 0.4, 0.8, and 1.2 s were performed and checked for positive cross-peaks. Only for the last case (where $d_2 > T_1$) were two positive cross-peaks identified as shown in Figure 9.

Electrochemistry. A computer-controlled system, consisting of a HEKA PG590 potentiostat (HEKA, Mahone Bay, NS, Canada), was used for the cyclic voltammetry experiments. Data were collected using a multifunction DAQ card (PCI 6251 M Series, National Instruments Austin, Texas) and in-house software written in the LabVIEW environment. Glassy carbon (BAS, 3 mm) was used as the working electrode. The quasi-reference electrode (QRE) was a silver wire ($E = 0.645$ V versus the formal potential, $E°'$, of 0.1 mM Fc/Fc^+). All electrochemical measurements were made using the QRE and subsequently rescaled to the ferrocene/ferrocenium formal potential.[35] A loop of gold wire was used as the auxiliary electrode. Before each measurement, a 1 mM solution of **3** was freshly prepared in dry thf with 0.1 M supporting electrolyte ([Bu_4N][PF_6], [Bu_4N][BF_4], or [Bu_4N][ClO_4]). Extra efforts were undertaken to remove moisture and oxygen from the solvent thf. The solvent was first dried using an MBraun solvent purification system and then filled into a 1 L flask, which was part of a specialty Schlenk line, equipped with greaseless Young valves. To the predried thf were added small amounts of 1,1-diphenylethylene and butyllithium, resulting in a red solution, which indicated the absence of moisture. By flask-to-flask condensation under reduced static pressure, a small amount of thf was condensed into a Schlenk tube from the thf reservoir flask. The inert gas (N_2 4.8) used for this Schlenk line was purified by conducting it through two columns before feeding it into the Schlenk line (one column equipped with a Cu(I) catalyst and one column equipped with 4 Å molecular sieves; both materials purchased from MBraun). A thus-prepared Schlenk tube filled with freshly condensed thf was moved into the glovebox. The electrolytes were dried under high vacuum ([Bu_4N][PF_6] overnight at 100 °C; [Bu_4N][BF_4] overnight at 70 °C; [Bu_4N][ClO_4] for 3 days at 25 °C). Unless otherwise specified, the scan rate for all CVs reported was 100 mV/s. All measurements were conducted inside a glovebox and taken at ambient temperature (24−25 °C).

Synthesis of Dichlorido{[(dimethylamino)dimethylsilyl]bis(trimethylsilyl)methyl-κ^2C,N}indium(III) (2a). MeLi (20.2 mL, 1.0 M in thf/cumene) was added to a solution of Me_2NtsiH (5.172 g, 19.80 mmol) in thf (10 mL), and the mixture was heated for 24 h at 45 °C. All volatile materials were removed in vacuo to leave a yellow solid behind. The solid was dissolved in Et_2O (30 mL), and the solution was added dropwise to a slurry of $InCl_3$ (4.205 g, 18.96 mmol) in Et_2O (20 mL) at 0 °C and subsequently stirred for 16 h. All volatiles were removed under vacuum from the resulting yellow solution to a give a yellow solid, which was then dried at 60 °C under high vacuum. The product was extracted with benzene (4 × 10 mL). The combined benzene phase was filtered, and the filtrate was reduced in volume to 20 mL and stored at 6 °C to yield colorless crystals (2.347 g). After the mother liquor was concentrated to 10 mL and stored at 6 °C, additional colorless crystals were obtained (0.496 g) (combined crystal fractions: 2.843 g, 34%). A single crystal for X-ray structural analysis was picked from the first fraction of crystals. ^{1}H NMR (C_6D_6, 500.13 MHz): δ 0.01 (s, 6H, $SiMe_2$), 0.31 (s, 18H, $SiMe_3$), 2.05 (s, 6H, NMe_2). ^{13}C NMR (C_6D_6, 125.76 MHz): δ 2.02 ($SiMe_2$), 6.51 ($SiMe_3$), 41.19 (NMe_2), one C obscured. MS (70 eV, EI+) *m*/*z* (%): 430 (30) [M^+ − Me], 250 (13), 230 (100) [$Me_2NSiC(SiMe_3)_2^+$], 207 (11), 201 (17) [$(Me_3Si)_2C(SiMe)^+$], 187 (38) [$(Me_3Si)_2CSiH^+$], 129 (36) [$C_5H_{13}Si_2^+$], 115 (19) [In^+], 102 (22) [$Me_2SiNMe_2^+$], 73 (69)

(32) Al-Juaid, S. S.; Eaborn, C.; Hitchcock, P. B.; Hill, M. S.; Smith, J. D. *Organometallics* **2000**, *19*, 3224–3231.
(33) Butler, I. R.; Cullen, W. R.; Ni, J.; Rettig, S. J. *Organometallics* **1985**, *4*, 2196–2201.
(34) Berger, S.; Braun, S. *200 and More NMR Experiments*, 3rd expanded ed.; Wiley-VCH: Weinheim, 2004; pp 430 and 445.
(35) Bard, A. J.; Faulkner, L. R. *Electrochemical Methods*, 2nd ed.; John Wiley & Sons, Inc.: New York, 2001.

[$SiMe_3^+$], 59 (38) [$C_2H_7Si^+$]. Anal. Calcd for $C_{11}H_{30}Cl_2InNSi_3$ (446.35): C, 29.60; H, 6.78; N, 3.14. Found: C, 29.73; H, 6.89; N, 3.09.

Synthesis of {[(Dimethylamino)dimethylsilyl]bis(trimethylsilyl)methyl-κ^2*C,N*}diiodidoindium(III) (2b). Li(thf)(Me_2Ntsi) (3.43 g, 10.1 mmol) dissolved in toluene (20 mL) was added dropwise to a slurry of InI_3 (5.00 g, 10.1 mmol) in toluene (30 mL) at 0 °C, and the mixture was stirred for 2 h. The red solution was filtered and reduced in volume to ~10 mL. At −25 °C colorless crystals of analytically pure **2b** were obtained (2.76 g, 43%). A single crystal for X-ray structural analysis was picked from this fraction. ^{1}H NMR (C_6D_6, 500.13 MHz): δ 0.03 (s, 6H, $SiMe_2$), 0.34 (s, 18H, $SiMe_3$), 2.06 (s, 6H, NMe_2). ^{13}C NMR (C_6D_6, 125.76 MHz): δ 3.27 ($SiMe_2$), 6.95 ($SiMe_3$), 43.20 (NMe_2), one C obscured. MS (70 eV, EI+) *m/z* (%): 347 (100) [$C_9H_{26}InNSi_3^+$], 203 (53) [$(Me_3Si)_2C(SiMeH_2)^+$], 115 (35) [In^+], 73 (55) [$SiMe_3^+$]. Anal. Calcd for $C_{11}H_{30}I_2InNSi_3$ (629.25): C, 21.00; H, 4.81; N, 2.23. Found: C, 21.82; H, 5.13; N, 2.16.

Synthesis of Bis{[(dimethylamino)dimethylsilyl]bis(trimethylsilyl)methyl-κ^2*C,N*}bis(μ-ferrocene-1,1′-diyl)diindium(III) (3). Compound **2a** (1.337 g, 2.995 mmol) was dissolved in toluene (15 mL) and chilled to −20 °C. A suspension of $[(LiC_5H_4)_2Fe]\cdot {}^2/_3$tmeda (0.826 g, 3.00 mmol) in toluene (15 mL) was added dropwise via tubing. After stirring for 2 h, the color of the solution had changed to red. Subsequently, the reaction mixture was filtrated and concentrated to 5 mL. Crystallization at −25 °C gave analytically pure **3** as red crystals (0.758 g, 45%). A single crystal for X-ray structural analysis was picked from this fraction. ^{1}H NMR (C_6D_6, 500.13 MHz): δ 0.21 (s, 6H, $SiMe_2$), 0.44 (s, 18H, $SiMe_3$), 2.04 (s, 6H, NMe_2), 4.43, 4.45 (s, 8H, C_5H_4). ^{13}C NMR (C_6D_6, 125.76 MHz): δ 3.26 ($SiMe_2$), 7.95 ($SiMe_3$), 42.19 (NMe_2), 70.41, 76.33 (C_5H_4), 77.88 (*ipso*-C, C_5H_4), one C is obscured. Low-temperature ^{1}H NMR (C_7D_8, 500.13 MHz, −30 °C): *anti* isomer: 0.42 (s, 12H, $SiMe_2$), 0.51 (s, 36H, $SiMe_3$), 1.93 (s, 12H, NMe_2), 4.36, 4.43, 4.45, 4.57 (s, 16H, Cp); *syn* isomer: 0.20 (s, 36H, $SiMe_3$), 0.23 (s, 12H, $SiMe_2$), 2.14 (s, 12H, NMe_2), 4.15, 4.28, 4.45, 4.53 (s, 16H, Cp). MS (70 eV, EI+) *m/z* (%): 1118 (5) [M^+], 857 (28) [$M^+ - C(SiMe_3)(SiMe_2NMe_2) - H$], 560 (74) [$(C_5H_5)Fe(C_5H_4)$-$In[C(SiMe_3)(SiMe_2NMe_2)]^+$], 544 (22) [$C_{20}H_{35}FeInNSi_3^+$], 300 (80) [$(C_5H_5)Fe(C_5H_4In)^+$], 261 (17) [$HC(SiMe_3)(SiMe_2NMe_2)^+$], 230 (100) [$Me_2NSiC(SiMe_3)_2^+$], 217 (59) [$SiHMe_2C(SiMe_3)_2^+$], 186 (75) [$(C_5H_5)_2Fe^+$]. Anal. Calcd for $C_{42}H_{76}In_2Fe_2N_2Si_6$ (1118.93): C, 45.08; H, 6.85; N, 2.50. Found: C, 45.09; H, 6.76; N, 2.27.

X-ray Structural Analysis for 2a, 2b, and 3. All measurements were made on a Nonius KappaCCD four-circle diffractometer using monochromated Mo Kα radiation (λ = 0.71073 Å) at −100 °C. An initial orientation matrix and cell were determined from 10 frames using ϕ scans (1° per frame, 20 s exposures per degree for a 10° rotation).[36] Data were measured using ω-scans.[36] Data reduction was performed with the HKL DENZO and SCALEPACK software.[36] Absorption corrections were applied (see Table 1). The structures were solved using direct methods (SIR-97)[37] and refined by full-matrix least-squares method on F^2 with SHELXL97-2.[38] The non-hydrogen atoms were refined anisotropically. Hydrogen atoms were included at geometrically idealized positions (C−H bond distances 0.95/0.98/1.00) and were not refined. The isotropic thermal parameters of the hydrogen atoms were fixed at 1.5 times for methyl hydrogen atoms in compounds **2a** and **3** and 1.2 times that of the preceding carbon atom for all other hydrogen atoms. The asymmetric unit of **2a** consists of two half-dimer units that are not crystallographically equivalent. The two half-dimers are structurally very similar. In the structure of **2b** the carbon atoms [labeled as C(5A), C(6A), C(7A), C(5B), C(6B), C(7B)] of the methyl groups attached to Si(3) were disordered over two positions. Geometrical (SAME) and rigid body restraints (DELU and SIMU) were used to model the disorder in SHELXL97-2.[38] The refined site occupancy factors are 0.61(3) [C(5A), C(6A), C(7A)] and 0.39(3) [C(5B), C(6B), C(7B)], respectively.

Crystallographic data for all of the structures in this article have been deposited with the Cambridge Crystallographic Data Centre, under CCDC 684585 (**2a**), 684586 (**2b**), and 684587 (**3**). Copies of this information may be obtained free of charge from The Director, CCDC, 12 Union Road, Cambridge CB2 1EZ, U.K. (fax, +44-1223-336033; e-mail, deposit@ccdc.cam.ac.uk; web, http://www.ccdc.cam.ac.uk).

Acknowledgment. We thank G. A. Orlowski (University of Guelph) and H.-B. Kraatz (University of Western Ontario) for their help with electrochemical measurements in the initial stage of the project. We thank the Natural Sciences and Engineering Research Council of Canada (NSERC Discovery Grant, J.M.), the Department of Chemistry, the Saskatchewan Structural Sciences Centre, and the University of Saskatchewan for their generous support. We thank the Canada Foundation for Innovation (CFI) and the government of Saskatchewan for funding of the X-ray and NMR facilities in the Saskatchewan Structural Sciences Centre (SSSC).

Supporting Information Available: Crystallographic data for **2a**, **2b**, and **3** in CIF file format; ^{1}H NMR spectra of **3** (C_6D_6; 25 °C and C_7D_8; −30 °C); CV of **3** and ferrocene (thf/0.1 M [Bu_4N][ClO_4]). This material is available free of charge via the Internet at http://pubs.acs.org.

OM800342E

(36) Otwinowski, Z.; Minor, W. In *Macromolecular Crystallography*, Part A; Carter, C. W., Sweet, R. M., Eds.; Academic Press: London, 1997; Vol. 276, pp 307−326.

(37) Altomare, A.; Burla, M. C.; Camalli, M.; Cascarano, G.; Giacovazzo, C.; Guagliardi, A.; Moliterni, A. G. G.; Polidori, G.; Spagna, R. *J. Appl. Crystallogr.* **1999**, *32*, 115–119.

(38) Sheldrick, G. M. *SHELXL97-2: Program for the Solution of Crystal Structures*; University of Göttingen: Germany, 1997.